EUROPEAN FUSION DEVELOPMENT AGREEMENT

EFDA–JET–CP(02)03/10

E. de la Luna, V. Krivenski, G. Giruzzi, C. Gowers, R. Prentice,
J. M.Travere, M. Zerbini and JET EFDA contributors

# Impact of Bulk Non-Maxwellian Electrons on Electron Temperature Measurements

# Impact of Bulk Non-Maxwellian Electrons on Electron Temperature Measurements

E. de la Luna[1], V. Krivenski[2], G. Giruzzi[2], C. Gowers[3], R. Prentice[3], J. M.Travere[2] , M. Zerbini[4] and JET EFDA contributors*

*[1]Asociación Euratom-CIEMAT, CIEMAT, Spain*
*[2]Association Euratom-CEA, CEA/DSM/DRFC, CEA-Cadarache, France*
*[3]Euratom-UKAEA Fusion Association, Culham Science Center, Abingdon, UK*
*[4]Associazione Euratom-ENEA sulla Fusione, C.R. Frascati, Frascati, Italy*
** See annex of J. Pamela et al, "Overview of Recent JET Results and Future Perspectives", Fusion Energy 2000 (Proc. 18th Int. Conf. Sorrento, 2000), IAEA, Vienna (2001).*

Pre-Print of paper to be submitted for publication in proceedings of the 17th Topical Conference on High Temperature Plasma Diagnostics, Madison, USA, 08 - 11 July, 2002

**ABSTRACT.**
In NBI+ICRF-heated high-temperature JET plasmas, electron cyclotron emission (ECE) spectra measured by the Michelson interferometer are inconsistent with the electron bulk distribution being Maxwellian. This conclusion follows from new, accurate modelling of the ECE spectra over the full measured frequency range, covering the first four harmonics of the cyclotron frequency. A model distribution function obtained by fitting a measured ECE spectrum reveals a distortion of the Maxwellian that is sharply localized at ~1.5 × thermal momentum. A consequence deduced from this distribution is that the electron temperature measured by JET's Thomson scattering diagnostic, which weighs the bulk electrons differently, should be lower than the ECE one in the spatial region where this distortion exists. This prediction appears to be confirmed by temperature profile comparisons showing that core Thomson scattering electron temperatures on JET are up to 20% lower than ECE values for plasmas with strong NBI+ICRF heating. The possibility of addressing experimentally the question of whether the plasma has a Maxwellian bulk is also discussed. This goal can be accomplished by observing the emission at different angles with respect to the magnetic field (oblique ECE). Simulations of oblique ECE spectra using the model distribution function obtained previously show an angular variation of the emission that is characteristic of the distorted bulk.

## I. INTRODUCTION

In magnetically confined plasmas, the electron temperature profile is typically determined using the electron cyclotron emission (ECE) and Thomson scattering (TS) diagnostics. Under good operating conditions for both diagnostics—high-enough electron density for TS measurements, optically-thick plasmas for ECE measurements—discrepancies between the TS- and ECE-measured temperatures are typically lower than 10%.

There are several possible causes for the existence of apparent temperature discrepancies between the two diagnostics:

i) different spatial and temporal resolutions, and different lines-of-sight of the plasma (possibly combined with inaccurate determination of the Shafranov shift): these causes can be eliminated by careful modelling.

ii) inaccurate calibration of the ECE diagnostic: this can be checked and corrected by use of dedicated discharges in which the magnetic field and the current are slowly ramped.

iii) low photon counts for the TS measurement: this, in principle, can be mitigated by sophisticated statistical analysis of the collected data, although—as this paper will point out—there may exist genuine physical effects that are completely missed by a formal analysis of the data.

This paper deals with a genuine cause for discrepancy between the temperatures measured by the two diagnostics. An implicit assumption of the measurements is that the electron distribution function is nearly Maxwellian in the range of energies to which each diagnostic is sensitive. For TS and ECE diagnostics, the probed electrons are typically low-energy electrons belonging to the bulk

of the distribution. As this paper will argue, this assumption is not necessarily true in the presence of strong auxiliary heating, when a sizeable amount of power is absorbed by bulk particles.

In the presence of non-Maxwellian bulks, TS and ECE temperatures reflect the average value of the inverse of the (perpendicular) slope of the electron distribution in the momentum space volumes probed by the two diagnostics (for JET high-temperature discharges discussed here, the energy range determining the TS temperature encompasses most of the corresponding ones determining the 1st and 2nd harmonic ECE core radiation temperatures). Since the two diagnostics weigh the bulk electrons differently, the measured temperatures need not coincide. In this case, it is worth stressing that the measured temperatures do not necessarily reflect the average kinetic energy of the electrons, which is an integral property of the distribution, but rather a local one (in momentum space), the slope at some characteristic momentum.

Systematic discrepancies between TS and ECE temperature profiles during strong NBI+ICRF heating were first observed on TFTR in the supershot regime[1,2]. No explanation was found for their appearance, and previous analysis [3]—although based on a physically sound idea—was inconclusive, and, with hindsight, not accurate enough. As this paper shows, systematic temperature discrepancies, which appear to be genuine, are observed also on JET under similar conditions. These findings motivate the analysis presented here. The search for the cause of the discrepancy will be based on the study of the full ECE spectra measured by the Michelson interferometer, which cover several harmonics of the electron cyclotron frequency (rather than on the difference between the two temperature profiles); specifically, on the property that electrons located at the same radial position but contributing to the measured emission at different harmonics have slightly different resonant momenta, which is also the idea at the basis of Ref. [3]. By comparing the emission at different harmonics, one can actually perform an energy scan of the bulk of the electron distribution, and determine whether the bulk is Maxwellian—and if it is not, determine its form. Once the bulk distribution is obtained from the ECE spectra, the corresponding TS temperature profile is derived, and this prediction can be checked against the experimental TS temperature profile.

The remainder of the article is organized as follows. In Sec. II, a brief description of the main diagnostic systems used for the measurements analysed in this paper is presented. The experimental observations are summarized in Sec. III. The non-Maxwellian electron distribution function determined from the fit to the ECE spectra, and the impact this distribution has on TS temperature measurements are discussed in Sec. 4. In Sec. 5, the emission at different angles with respect to the magnetic field (oblique ECE) is considered to illustrate a direct method—which could be used on JET—for diagnosing distribution functions with non-Maxwellian bulks. Conclusions are presented in the final section.

## 2. EXPERIMENTAL SET-UP

The main electron temperature profile diagnostics in JET are Thomson scattering, using the LIDAR (light detection and ranging) technique, and second harmonic ECE. The LIDAR Thomson scattering

[4] yields a measurement of the electron density and temperature profiles each 0.25s with a radial resolution of 12cm. The backscattered light is collected from the low-field side, along a major radius close to the plasma equatorial midplane. ECE is measured by two different instruments: an absolutely calibrated Michelson interferometer and a 48-channels heterodyne radiometer. The Michelson interferometer measures the ECE spectrum over several harmonics (50 to 500GHz, X mode) with a spectral resolution of ~ 9GHz and a moderate temporal resolution (15ms), whereas the radiometer, with higher temporal resolution (~0.2ms) and covering the second harmonic frequency range (or the first harmonic depending on the magnetic field), is mainly used to monitor the temporal evolution of the electron temperature profile. The radiometer is cross-calibrated to the Michelson interferometer during the ohmic phase of the discharge. A detailed description of the design and performance of both systems can be found in [5, 6]. Both instruments view the plasma from the low-field side by means of two antennas in the form of oversized waveguides ($50 \times 65$ mm) located at heights of 0.35 and 0.133m (for the Michelson interferometer and the radiometer respectively). Since for typical JET configurations the center of the plasma is displaced upwards by typically 0.3 to 0.4 m, the Michelson line of sight is generally very close to the plasma center. In the case of ECE measurements, the characteristics of the receiving optics (the divergence of the antenna pattern) determine the spatial resolution transverse to the line of sight, while the spatial resolution along the line of sight is determined by the frequency resolution of the detection system and line broadening effects of the emission.

## 3. COMPARISON BETWEEN ECE AND THOMSON SCATTERING DATA

On JET, electron temperature profiles are measured simultaneously by second harmonic ECE and LIDAR Thomson Scattering. A good agreement is generally observed between these two independently calibrated diagnostics for ohmic plasmas, as expected for black-body emission by thermal plasmas. This point is illustrated in Fig.1 where a comparison between central temperature values derived from ECE and TS is shown. This comparison includes magnetic field ramp calibration shots [7], which are routinely performed at the beginning of each experimental campaign on JET in order to check the absolute calibration of the Michelson interferometer, and high-density plasmas heated with NBI. The main parameters scanned are the density ($10^{19}$ m$^{-3}$< $n_e(0) < 8 \times 10^{19}$ m$^{-3}$), the magnetic field ($2.4 < B_0 < 3.4$T), and the heating power ($1 < P_{NBI} < 15$MW), which results in temperature variations in the range of $T_e(0) < 6$keV. Due to the different spatial resolution of the two diagnostics, the data plotted in the figure are obtained by averaging the temperature values over ± 0.1m around the magnetic axis for both profiles. The spread of the data around the equality line not only reflects the systematic error in the spectral calibration of the Michelson interferometer, which is estimated to be ~10 % in absolute value and ~5% in relative shape [7], but it is also affected by the type of discharge evolution since the two instruments have very different time resolution. Figure 2 shows a similar comparison but in this case for a number of combined ICRF and NBI heated discharges. The database contains central temperature values of more than 40 discharges heated by

a combination of NBI ($P_{NBI}$ < 18MW) and ICRH ($P_{ICRH}$ < 8MW), with magnetic fields ranging from 2.6 to 3.5T and central electron densities from $2\times10^{19}$ to $6\times10^{20}$ $m^{-3}$. The ICRH system uses the fundamental hydrogen minority heating scheme with the resonance located near the plasma center. Plasmas with 5 - 8MW of ICRH reach peak electron temperatures, as measured by ECE, higher than 6keV. In general, it is observed that increasing the ICRH power results in a higher central $T_e$, and in an increase of the peaking of the temperature profile.

As shown in Fig.2, although there is still a relatively good agreement between the two diagnostics for temperatures below 5 keV, above that value the electron temperature deduced from ECE measurements appears to be systematically higher (up to 20%) than the one measured by Thomson scattering. The deviation from the equality line in the case of ECE temperature higher than 6keV is well above the usual LIDAR statistical error of ~7%. An example of the temperature profiles measured with the two diagnostics, in a discharge where strong auxiliary heating power is applied, is shown in Fig.3. It is interesting to note that the disagreement between the diagnostics appears only in the central part of the plasma, where the optical thickness of the plasma is very large and the electron density higher.

## 4. ECE SIMULATIONS

In order to gain a further insight into the possible causes of the observed discrepancy between ECE and TS core temperatures, detailed simulations of the ECE spectra have been carried out. For this purpose a fully relativistic radiation code [8] has been used to evaluate the local emission and absorption coefficients, and the total emitted radiation. Reflections, both at the walls and at the cut off layer, and depolarisation of the radiation due to wall reflection [9, 10] are included in the analysis (and described by coefficients $\Gamma$, $\Gamma_c$ and $\Pi$ respectively), as well as the instrumental effects and the effect of the antenna pattern in both toroidal and poloidal directions.

We first consider the ohmic case. Figure 4 shows typical spectra measured on JET by the Michelson interferometer during the ohmic phase of two discharges at different magnetic fields, together with the corresponding computed spectra assuming a Maxwellian distribution function. As input data to compute the spectra, we use the magnetic field profile and the location of the flux surfaces obtained from plasma equilibrium reconstruction done using EFIT [11], and the $n_e$ profile measured by TS. In ohmic plasmas, the $T_e$ profile derived from the 2nd harmonic frequency range of the ECE spectrum is typically in agreement with the one measured by TS. As it can be seen from Fig.4, the computed spectra closely match the measured ones, including the peak corresponding to the 1st harmonic depolarized O mode, giving us an estimate of the accuracy with which the radiation code is able to reproduce the experimental observations.

A similar analysis was repeated for a high-$T_e$ discharge on JET ($P_{ICRH}$ = 5MW and $P_{NBI}$ = 15.7 MW). The main conclusions deduced from this analysis are summarized in Fig.5, where the measured spectrum is shown together with three different fits computed with: a), b) a Maxwellian distribution function obtained by fitting the range of frequencies resonant at the 2nd harmonic (red) or the one

resonant at the 3rd harmonic (green), and c) a model distribution function inferred from a consistent fit to the complete measured spectrum (blue). This analysis has revealed that, under those plasma conditions, the temperature profile deduced from the 2nd harmonic emission is inconsistent with that deduced from the 3rd harmonic [12]. This observation implies that the bulk of the distribution function is not well described by a Maxwellian, since, in high-Te plasmas on JET, the 3rd harmonic emission is also optically thick, and therefore provides an independent measurement of the bulk electron temperature but related to electrons with higher energy [3, 8]. The good agreement obtained between experimental data and simulations for the ohmic cases (see Fig.4) is a clear indication that errors in the absolute calibration of the Michelson interferometer can not be the cause of the observed anomaly in the measured spectrum.

Figure 6 shows the model distribution function determined from the ECE spectrum in Fig.5, and the Maxwellian distribution function (unperturbed Maxwellian) that is obtained from an intermediate fit to both 2nd and 3rd emission and is the "best Maxwellian fit" of the spectrum [12]. Also plotted in this graph are the average momentum of the electrons that contribute to the detected ECE at different harmonics s , and the momentum range corresponding to the spectra measured by the TS diagnostic on JET. The main feature of the model distribution function is the flattening that appears in the low-energy range of the distribution, which is sharply localized at u/uth <1.5 ($u_{\mathrm{th}}$ is the thermal momentum), this property being determined by the fit to the 1st and the 2nd harmonic emission. The distribution function is assumed to be Maxwellian for $\rho > 0.35$.

We now consider the effect of the model distribution function determined from the ECE spectrum on TS measurements. Figure 7 shows the computed TS spectrum, for $\rho = 0$, using the model distribution function, and the fit to that spectrum performed using a Maxwellian (see also Fig. 6), illustrating the typical procedure followed to determine the value of the TS temperature. The experimental temperature values measured by TS and the computed temperature profile using the model distribution function are shown in Fig.8. The kinetic temperature derived from the model distribution function and the temperature profile obtained from the 2nd harmonic ECE are also plotted in the figure. The agreement found between the computed and measured TS profiles close to the plasma axis, although remarkable, might be of modest relevance, because more TS data should be fitted in order to obtain a statistically significant conclusion. The important point, however, is that the existence of a non-Maxwellian bulk distribution function implies that the TS temperature should be lower than the ECE temperature, effect that seems to be statistically confirmed in ICRF+NBI heated discharges on JET. Again, this fact can be easily understood by considering that the temperatures measured by the two diagnostics correspond to different integrals in momentum space over the distribution function (see Fig. 6).

## 5. OBLIQUE ECE

Up to this point, we discussed ECE normal to the magnetic field—which is the set-up typically employed for measuring the electron temperature. We saw how multiharmonic spectra measured

normally to the magnetic field can also be used to obtain information on the electron distribution, by using the property that the average resonant energy of the emitting electrons changes—in discrete steps—with the harmonic number. In this section, we consider the continuous variation of the resonant energy of the emitting electrons with changes of the observation angle that allows selecting the radiation $N_{||}$. We call this experimental set-up oblique ECE.

Figure 8 shows that, for finite and not too large values of the observation angle, the intrinsic spatial resolution of oblique ECE given by the line-shape factor is good, and comparable to that of normal emission. The range of observation angles $|\psi| < 20°$ corresponds to an energy range of the emitting electrons that spans the whole bulk of the electron distribution for typical JET parameters, as shown in Fig. 9 for the 2nd harmonic emission (the effect on the other harmonics is qualitatively similar). The change in resonant energy with $N_{||}$ is due to a change in both the parallel and perpendicular energy of the emitting electrons, the sign of $N_{||}$ selecting the sign of $u_{||}$ of the resonant electrons: thus a scan in $N_{||}$ provides a 2D scan of the electron distribution function in momentum space; this, combined with a frequency scan that gives the radial dependence (and through emission at different harmonics improves the perpendicular energy resolution), provides a 3D image of the electron distribution in phase space.

These attractive properties of oblique ECE generated early interest for the study of LH-induced electron tails, both theoretically [13, 14]—it was shown that oblique ECE contains enough information to reconstruct the tail of electron distribution, and experimentally [15, 16]—three Michelson interferometers, measuring radiation with three different values of $N_{||}$, were installed on Tore Supra; unfortunately, this experiment was prematurely terminated. Oblique ECE measurements were also carried out on PBX [17, 18], although in a different regime—in cold, small, and dense plasmas, at weak magnetic fields—in which the information provided by the diagnostic is much weaker.

Oblique ECE is also sensitive to distortions of the bulk of the distribution [19]. In order to study effects similar to the ones discussed here but induced by central electron cyclotron heating, an oblique ECE diagnostic was installed on FTU recently [20].

Simulated oblique ECE spectra are presented in Fig.10 for JET parameters, comparing the case in which the electron distribution is Maxwellian to the case discussed in the previous section where the bulk distribution function is distorted. Emission at the 2nd harmonic, in the case of a Maxwellina distribution (Fig. 11a), shows only the characteristic Doppler shift that moves the $T_{rad}$ maximum towards higher frequencies for increasing values of $|N_{||}|$. The distortion of the bulk causes an additional wiggling of the $T_{rad}$ maximum to appear, corresponding to the change of the slope of the distribution function as the average resonant energy of the emitting electrons increases. Preliminary measurements on FTU appear to support the existence of this qualitative and distinctive feature of oblique ECE in the presence of non-Maxwellian bulks [21].

## SUMMARY AND DISCUSSION

In conclusion, we have shown that the detailed analysis of ECE spectra extending over several

harmonics of the cyclotron frequency is a powerful method not only for measuring the temperature profile, but also for obtaining information about the shape of the electron distribution function. In the case of strong auxiliary heating on JET, simulations of the measured ECE spectra point to the existence of a distortion of the bulk of the distribution function. The calculations also show that, under those conditions, the temperature values measured by TS and ECE do not need to coincide, prediction that appears to be supported by experimental evidence. A major point that remains to be addressed is what are the physical processes that cause the appearance of non-Maxwellian bulks in high-$T_e$ plasmas. Fokker-Planck calculations suggesting the existence of a distortion in the bulk of the distribution function during high-power on-axis ECRH experiments on FTU were reported recently [22]. Hence, one may speculate that non-Maxwellian bulk distribution functions can appear in plasmas with a high level of auxiliary power whenever a sufficient amount of heating power is absorbed by the bulk.

The analysis of the experimental conditions for which such a type of phenomena is observed on JET can give us a hint of the responsible mechanism. The signatures of the existence of a non-Maxwellian bulk, i.e., discrepancies between TS and ECE temperatures and/or the characteristic anomaly in the ECE spectra, have been identified during NBI+ICRF heating experiments, and also during the alpha heating experiments carried out on JET [23].

In both scenarios, since ICRF heating is tuned to the hydrogen minority resonance, a high-energy ion tail develops that extends into the mega-electronvolt energy range. This implies that in these cases the distortion of the bulk of the distribution function could result from the interaction of high-energy ions with thermal electrons. Discrepancies between TS and ECE temperature measurements have also been observed to occur on JET when the main heating phase of the discharge includes LH heating in combination with NBI and ICRH. The presence of an energetic LH-driven electron tail, however, produces harmonic-overlap in the emitted spectrum, and makes the interpretation much more laborious. Analysis of this type of discharges was also performed and will be reported elsewhere.

Finally, it has been shown that the measurement of multiharmonic ECE spectra at different angles with respect to the magnetic field is an attractive method to identify deviations from the Maxwellian distribution function. Simulations indicate that, by using this technique, a complete phase-space measurement of the electron distribution function would be possible, providing information that might be essential for the understanding of the physics of high-temperature plasmas.

## REFERENCES


[1]. G. Taylor, J. R. Wilson, et al., Plasma Phys. Contr. Fusion **36** (1994) 523.

[2]. G. Taylor, et al., Proc. of the 9th Joint Workshop on ECE and ECH, Borrego Springs, (World Scientific, 1995) 485.

[3]. I. Fidone, G. Giruzzi and G. Taylor, Phys. Plasmas **3** (1996) 2331.

[4]. C. W. Gowers, B. V. Brown et al., Rev. Sci. Instrum. **66** (1995) 471.

[5]. D. V. Bartlett, et al, Proc. of the 6th Joint Workshop on ECE and ECRH, Oxford (1987)

[6]. D. V. Bartlett, C. Bishop, R. Cahill, A. McLachlan et al., Proc. of the 9th Joint Workshop on ECE and ECRH, Borrego Springs (1995)
[7]. H. Bindslev and D. Barlett. JET-Report R(88) 04.
[8]. V. Krivenski, Proc. of the 12th Joint Workshop on ECE and ECRH, Aix-en-Provence (2002)
[9]. A. E. Costley, R. J. Hastie, J. W. M. Paul, and J. Chamberlain, Phys. Rev. Lett. 33 (1974) 758.
[10]. A. E. Costley and TFR Group, Phys. Rev. Lett. 38 (1977) 1477.
[11]. L. L. Lao, H. St. John, R. D. Stambaugh, A. G. Kellman, and W. Pfeiffer, Nuclear Fusion 25 (1985) 1611.
[12]. V. Krivenski, E. de la Luna, G. Giruzzi, et al., Proc. of the 29th EPS Conf. Contr. Fusion and Plasma Physics, Montreux, **26B** (2002) O-1.03.
[13]. V. Tribaldos and V. Krivenski, Proc. of the 8th Joint Workshop on ECE and ECRH, Gut-Ising (1992) (Max-Planck Institut für Plasma Physik, Germany, 1993) Rep. No. IPP III/186, Vol. 1, 123.
[14]. V. Krivenski and V. Tribaldos, Proc. of the 20th EPS Conf. on Contr. Fusion and Plasma Physics, Lisbon, **17C-II** (1993) 1045.
[15]. L. Rodríguez, N. Augé, et al, Proc. 18th EPS Conf. Contr. Fusion and Plasma Physics, Berlin, **15C-IV** (1991) 353.
[16]. M. Talvard, G. Giruzzi and W. D. Liu. Proc, 19th EPS Conf. Contr. Fusion and Plasma Physics, Innsbruck, **16C-II** (1992) 1103.
[17]. S. Preische, P. C. Efthimion, and S. M. Kaye, Phys Plasmas **3** (1996) 4065.
[18]. S. Preische, P. C. Efthimion, and S. M. Kaye, Rev. Sci. Instrum. **68** (1997) 409.
[19]. V. Krivenski, Proc. of the 11th Joint Workshop on ECE and ECRH, Fusion Eng. Des. **53** (2001) 23.
[20]. O. Tudisco, E. de la Luna, V. Krivenski, et al, Proc. of the 28th EPS Conf. on Contr. Fusion and Plasma Physics, Madeira (2001).
[21]. E. de la Luna, V. Krivenski, O. Tudisco, et al, Proc. of the 12th Joint Workshop on EC and ECH, Aix-en-Provence, 2002.
[22]. V. Krivenski, G. Bracco, P. Buratti, G. Giruzzi, O. Tudisco, S. Cirant, and F. Crisanti, submitted for publication.
[23]. P. R. Thomas, P. Andrew, B. Balet, D. Bartlett, et al., Phys. Rev. Lett. **80** (1998) 5548.

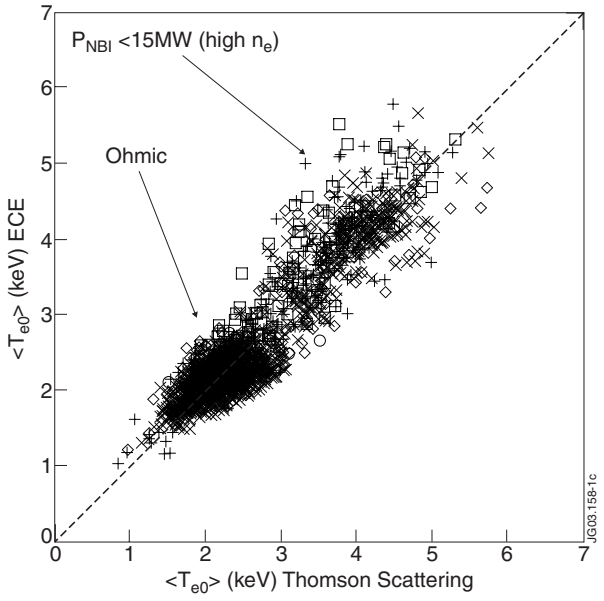


*Figure 1: Comparison between central temperatures measured by Thomson scattering (LIDAR) and ECE (Michelson interferometer, 2nd harmonic, X mode), for ohmic plasmas and high-density plasmas heated with NBI ($P_{NBI}$ < 15MW), and different values of the toroidal field (2T < $B_0$ < 3.4T)*

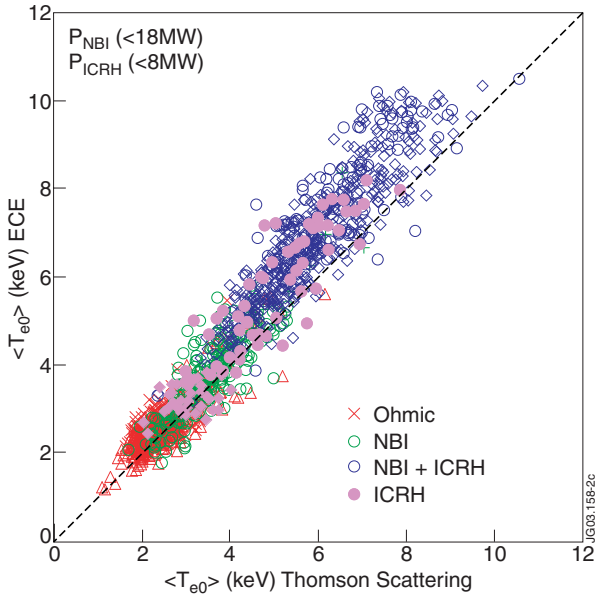


*Figure 2: As in Fig. 1, for plasmas with different types of additional heating.*

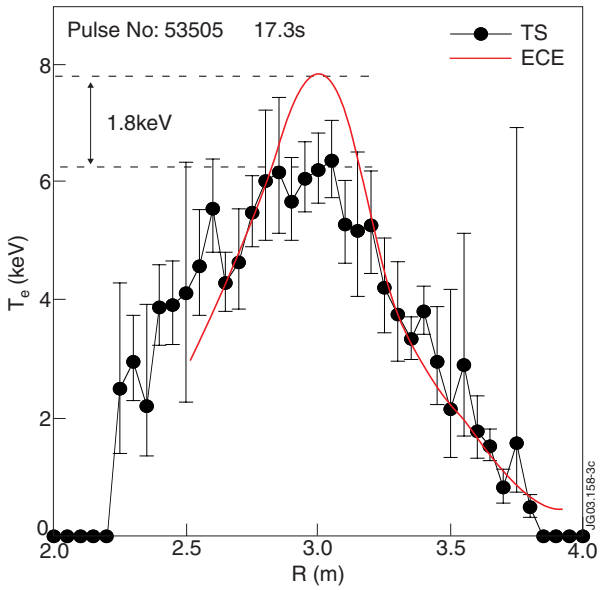


*Figure 3: Electron temperature profiles measured by Thomson scattering (LIDAR) and ECE (Michelson interferometer, 2nd harmonic, X mode) for a plasma with ICRF+NBI heating ($P_{ICRH}$ = 5MW, $P_{NBI}$ = 3MW), showing the disagreement existing between the two measurements in the plasma core during strong auxiliary heating.*

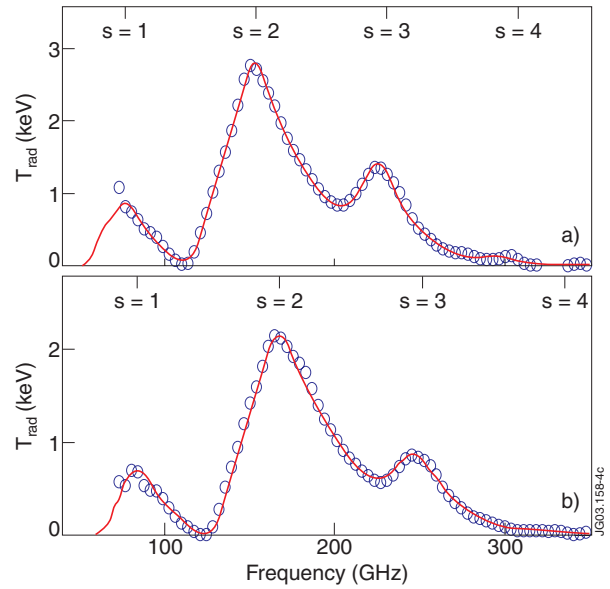


*Figure 4: Typical X-mode ECE spectra measured by the Michelson interferometer (symbols) during the ohmic phase of a discharge, and the corresponding simulated spectra (full lines) assuming a Maxwellian distribution function, for the plasma parameters:*
*a) $B_0$ = 2.78T, $n_e$ (0)= 1.85 × $10^{19}$ $m^{-3}$;*
*b) $B_0$ = 3.04T, $n_e$ (0) = 1.98 × 1019 $m^{-3}$.*
*In both cases the reflection coefficients used to compute the spectra are Γ = 0.65, $Γ_c$ = 0.80, and Π = 0.32. The top scale gives the harmonic number, s, for on-axis resonant electrons.*

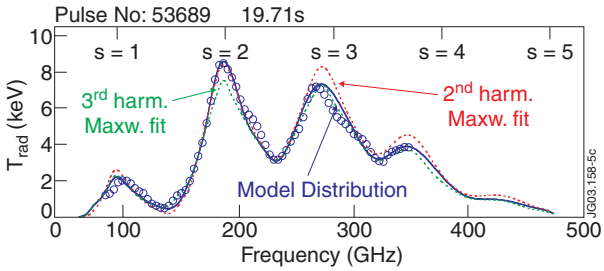


*Figure 5: Spectrum of the radiation temperature (X mode) measured by the Michelson interferometer (symbols) during ICRH + NBI heating ($P_{ICRH}$ = 5MW, $P_{NBI}$ = 15.7MW). The dashed lines represent the emission from a Maxwellian distribution obtained by fitting the range of frequencies resonant at the 2nd harmonic (red) or the one resonant at the 3rd harmonic (green), and the full line corresponds to a consistent fit to the experimental spectrum (blue). To obtain the latter fit, a Maxwellian distribution function is perturbed by flattening (steepening) its slope at momenta corresponding to electrons emitting at the 2nd harmonic (at the 1st, 3rd, and 4th harmonics); see also Fig. 6. The distribution function is assumed to be Maxwellian for ρ > 0.35. The plasma parameters are: $B_0$ = 3.4T, $n_e$ (0)= 3.3 × $10^{19}$ $m^{-3}$.*

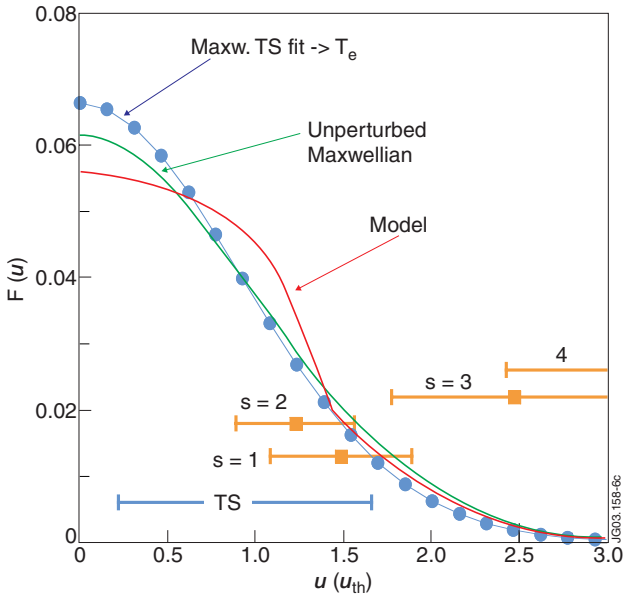


*Figure 6: Maxwellian distribution function (green) obtained by an intermediate fit to both the 2nd and 3rd harmonic emission of the spectrum shown in Fig. 5, and the model distribution function (red) that gives the correct fit to the full spectrum plotted in Fig. 5. The horizontal bars give the average momentum of the emitting electrons (±1 standard deviation) at ρ = 0, for each harmonic s [$u = p/u_{th}$, $u_{th} = (m_e T_e)^{1/2}$], and the energy range of the TS diagnostic on JET. The Maxwellian distribution derived from the fit to the Thomson scattering spectrum presented in Fig. 7 is also shown (symbols).*

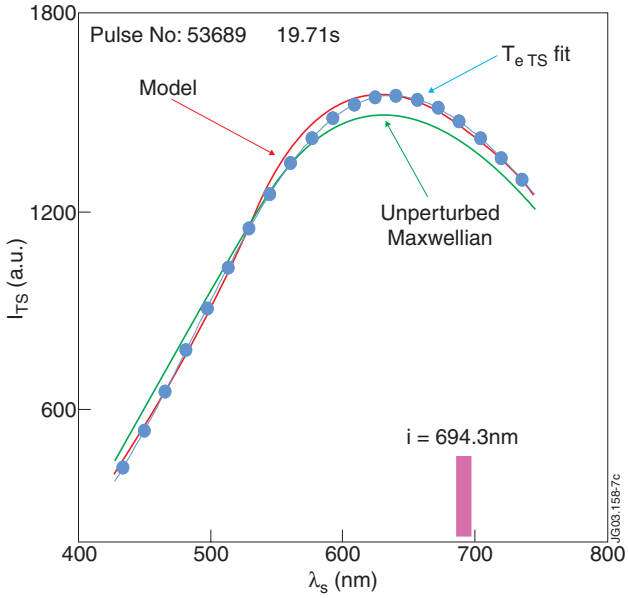


*Figure 7: Computed Thomson scattering spectra from the distribution functions shown in Fig. 6; the Maxwellian fit to the model-distribution spectrum (filled circles) mimics the procedure used in practice to determine the value of the TS temperature.*

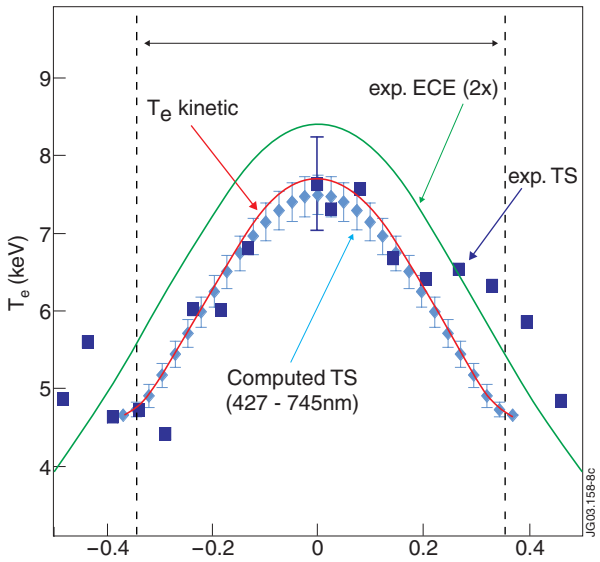


*Figure 8: Computed Thomson scattering temperature profile (diamonds) from the model distribution function, see Fig. 6 (the computed errors bars are not of statistical nature but due to the non-Maxwellian form of the fitted TS spectra). The profile corresponding to the average kinetic energy of the model distribution and the measured temperature profiles (exp.) are also shown. The experimental TS data points are shifted, $\rho \rightarrow \rho - 0.06\,(1-\rho^2)$, in order to correct the EFIT-determined Shafranov shift with the one obtained from the fit to the ECE spectrum.*

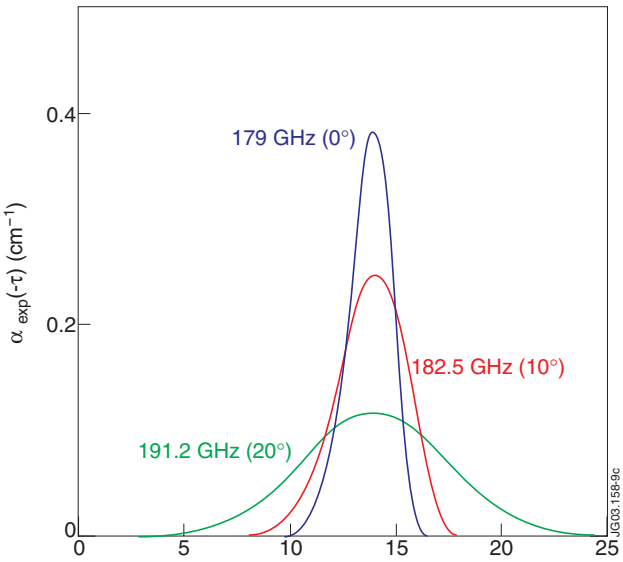


*Figure 9: Shape factor determining the spatial localization of the emission at different frequencies and observation angles, for the plasma parameters of Fig.5. The observation angle is given with respect to the normal to the magnetic field.*

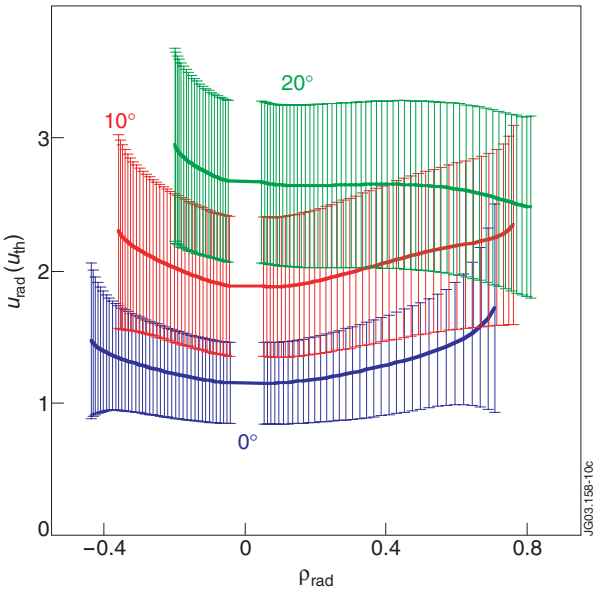


*Figure 10: Average momentum of the emitting electrons in the X mode at 2nd harmonic (±1 standard deviation) for different observation angles. Plasma parameters as in Fig. 5.*

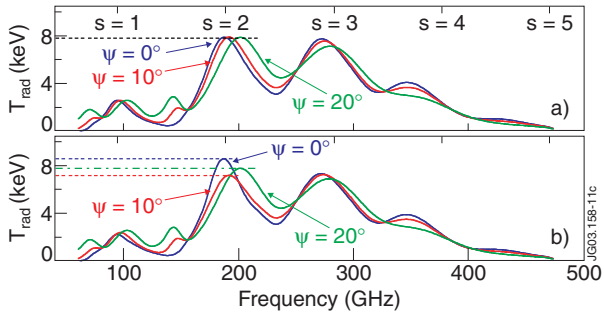


*Figure 11: Computed spectra of the radiative temperature in the X mode for different observation angles: (a) for a Maxwellian ($T_{e0}$ = 8.2keV), and (b) for the model distribution function shown in Fig.6. Plasma parameters as in Fig.5.*